Pore size distribution, porosity and permeability of saturated kaolin along triaxial stress paths

Qian-Feng GAO[1], Mohamad JRAD[1], Mahdia HATTAB[1] , Lamine IGHIL AMEUR[1]

1. Laboratoire d'Etude des Microstructures et de Mécanique des Matériaux, CNRS UMR 7239, Université de Lorraine, Ile du Saulcy, 57045 Metz Cedex 01, France

Abstract: The aim of this work was to identify the pore structure and permeability of clay under various triaxial loading. Triaxial tests were conducted on saturated kaolin specimens, and mercury intrusion porosimetry (MIP) and scanning electron microscopy (SEM) were subsequently adopted to analyze the local pore properties. An improved permeability model was proposed and then used to predict the permeability of kaolin based on MIP results. The influences of the over consolidation ratio (OCR) and the stress path on pore structures and permeabilities were observed. The proposed model is approved to be capable of predicting the permeability of clay with some desirable advantages.

Keywords: pore size distribution; porosity; permeability; kaolin; mercury intrusion porosimetry

1 Introduction

Pore structure is one of the most important microstructural properties of clay. The most common method for the measurement of microscopic pore properties is to perform MIP tests. The other methods include the nitrogen adsorption isotherm method, the microscopic image analysis and the X-ray microtomography. Pore structural properties directly determine many physical properties of soil, especially the permeability. An accurate acquisition of clay permeability from the experiments or from permeability models has been a challenging task (Leonards, 1962). Fortunately, plenty of microscopic experiments have confirmed that the pore structure essentially controls the soil permeability. This has prompted many researchers to focus on the correlation between soil permeabilities and pore structural parameters (Garcia-Bengochea et al., 1978, 1979; Lapierre et al., 1990).

Although a lot of experimental studies on soil pore structure have been carried out, it is still not clear how the pore structure varies under different triaxial loading. Moreover, none of the existing permeability models gives a general relationship between pore properties and permeability that would be valid for various clay materials. The objective of this work is to investigate the pore structural properties of clay under different stress paths and OCRs, and to develop a more general model for clay permeability. Therfore, triaxial CD tests followed by MIP tests and SEM observations were carried out on kaolin specimens. An improved permeability model based on MIP results was proposed and verified. The pore properties and permeabilities under different stress paths and OCRs were analyzed.

2 Materials and methodology

2.1 Material properties and triaxial tests

The material studied is kaolin K13. Its liquid and plastic limits are w_L = 41.6% and w_P = 21.2%. The specific gravity of the solids is $G_s = \gamma_s/\gamma_w$ = 2.63 and the specific area of the clay is 27 m^2/g.

Specimens were prepared from kaolin K13 slurry with $w_{ini} = 1.5\ w_L$. The slurry was firstly uniaxial consolidated under a vertical stress of 120 kPa. Afterwards, cylindrical specimens with a height of 75 mm and a diameter of 50 mm were extracted for triaxial CD compression tests. After saturation, isotropic consolidation was applied by increasing p' to the target value p_1' under drained condition for

normally consolidation tests. In the over consolidation tests, p' was firstly increased to p_0' = 1000 kPa and then reduced until the desirable OCR= p_0'/p_1' was obtained. Subsequently, q or/and p' was applied to the specimens along the conventional constant σ'_3 stress path or the purely deviatoric stress path, to meet the same stress level at p'_2 = 300 kPa, q_2 = 150 kPa in the (p', q) plane.

Table 1 Triaxial tests on remolded saturated kaolin specimens

Specimens	Stress path	e_{00}	p_0'	p_1'	OCR	e_0	$\eta_f = q_f/p'_f$	e_f
NC_P300	P	0.893	/	300	1.0	0.758	0.53	0.738
NC_S250	S	0.921	/	250	1.0	0.790	0.50	0.766
OCR3.3_P300	P	0.966	1000	300	3.3	0.727	0.53	0.741
OCR4.0_S250	S	0.809	1000	250	4.0	0.608	0.61	0.604

Notes: S represents the constant σ'_3 stress path and P represents the purely deviatoric stress path; e_{00} is the void ratio after uniaxial consolidation; e_0 is the void ratio before triaxial shearing; p'_f and q_f are the final effective mean stress and the final deviatoric stress; e_f is the void ratio at the end of triaxial shearing.

2.2 Methods used for microstructural observations

After triaxial testing, specimens were recovered from the cell and cut into subsamples for MIP tests and SEM observations. MIP samples were freeze-dried and then mounted in the mercury filled sample cups in a pressure vessel. The pressure was slowly increased to about 206 MPa, which corresponded to a pore-throat diameter of 6 nm (contact angle θ = 147° and surface tension γ = 0.484 N/m). By MIP tests, the cumulative volume curves and differential volume curves of pores were directly acquired.

The freeze-drying method was also adopted to dehydrate SEM subsamples. The vertical fresh planes (parallel to the axial stress) used for SEM observation were obtained by fracturing the frozen subsamples and vacuum coated with thin layers of gold after drying. SEM images were taken at several typical areas on the vertical plane of every sample. An image processing method based on ImageJ software was used to examine 2D pore parameters. To predict 3D pore diameters from 2D results, the 25F association method proposed by Xu and Pitot (2003) was employed.

3 A improved model for permeability prediction

From Hagen-Poiseuille's equation, Leonard (1962) deduced an equation for permeability of parallel and circular capillaries with identical diameters:

$$k = \frac{\gamma_w n}{32\eta_w} D^2 \tag{1}$$

where k is the coefficient of permeability; γ_w is the specific weight of water; n is the porosity; D is the diameter of the capillary; η_w is the dynamic viscosity of water.

To consider the pore size distribution (PSD), we improved this model by replacing n and D with n_* and D_* respectively:

$$n_* = e_* / (1 + e_*) \tag{2}$$

$$D_* = c \cdot D_e \tag{3}$$

where e_* is the void ratio obtained from MIP test; c is a non-dimensional correction factor; D_e is the expected value of pore diameter. c and D_e can be calculated from the following equations:

$$c = \sqrt{\frac{\mu + 3}{m \cdot \sigma}} \tag{4}$$

$$D_e = 10^{\mu} \tag{5}$$

$$\mu = \sum_i f(D_i) \cdot \log D_i \tag{6}$$

$$\sigma = \sqrt{\sum_i (\log D_i - \mu)^2 \cdot f(D_i)} \tag{7}$$

where m is a constant; μ is the expected value of logD_i; σ is the standard deviation of logD_i; $f(D_i)$ is the probability density at logD_i, which can be determined from the differential volume curve.

Fig. 1 presents two examples of permeability prediction based on the MIP test results in Garcial-Bengochea et al. (1978) and Lapierre et al. (1990). One can note that the model proposed in this paper is capable of predicting the permeability of fine-grained soils. One obvious advantage of the new model is that its form does not change with soils (silt-kaolin mixtures, remoulded and intact Louiseville clay) and even the only constant m is kept the same (m=25 for the cases in Fig. 1).

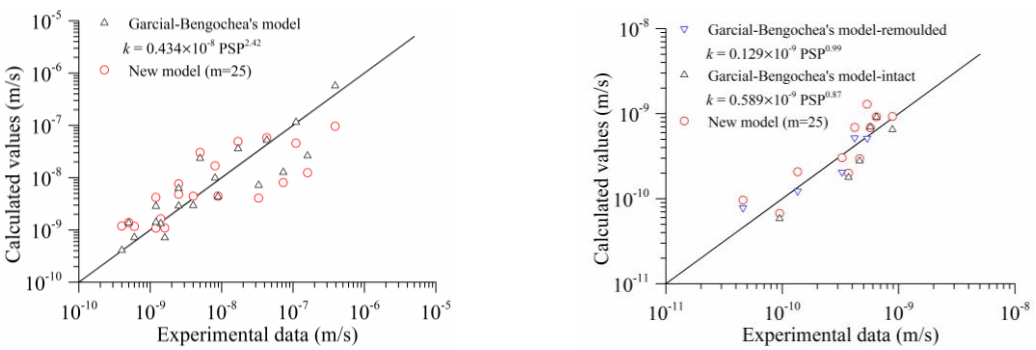

(a) silt-kaolin mixtures (b) Louiseville clay

Fig. 1 Verification of the proposed permeability model

4 Pore properties and permeabilities of clay under triaxial loading

4.1 PSD and void ratio obtained from MIP and SEM

As shown in Fig. 2, the two normally consolidated specimens had nearly the same cumulative pore volumes concerning a given method. Whereas, a large difference between those of the two over-consolidated specimens was observed. These results were in agreement with the conventional experimental data (Table 1). One can note that the void ratios, e_{MIP}, measured by MIP were visibly less than e_f due to the fact that the mercury cannot be intruded into the closed pore space within specimens. Additionally, the pore volumes measured by MIP were about two times greater than those obtained from SEM, although a similar changing tendency between them was observed.

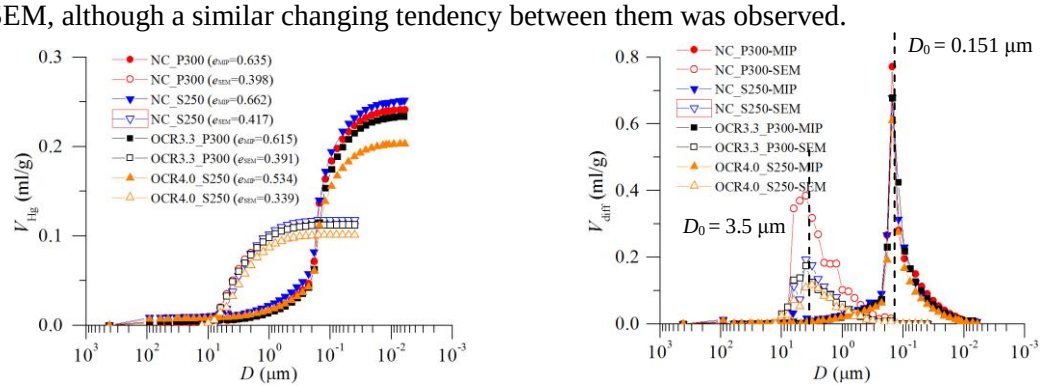

(a) (b)

Fig. 2 Pore volume derived from MIP and SEM: (a) cumulative volume; (b) differential volume

The differences between the results of MIP and SEM can be explained from their different basic principles. The pore diameter measured by MIP corresponded to that of the entrance of pores, whereas

the diameter of pores in SEM images was equivalently estimated from circles. On the other hand, the latter was primarily based on 2D images, whose results could not accurately reflect 3D pore structures although a 2D-to-3D prediction method was adopted. Additionally, too small or too large pores were neglected in the SEM method. All the specimens had approximately the same modal pore diameter, D_0, of 0.151 μm by MIP tests, compared to that around 3.5 μm by SEM image processing. However, it is observed that the differential volume curves of the specimens along the constant σ'_3 stress path had lower kurtosis than those of the specimens following the purely deviatoric stress path (Fig. 2b).

4.2 Predicted coefficients of permeability using MIP results

Table 2 gives the predicted coefficients of permeability of four specimens using the proposed permeability model (m=25). One can note that the coefficients of permeability of the normally consolidated specimens were larger than those of the over-consolidated specimens. On the other hand, the coefficients of permeability of the specimens along the purely deviatoric stress path were smaller than those of the specimens following the constant σ_3' stress path. Therefore, both the stress history (OCR) and the stress path affect the coefficient of permeability of clay, and these phenomena can well be characterized by the permeability model proposed in this paper.

Table 2 Predicted coefficients of permeability of four specimens

Specimen	n_{*1} (%)	n_{*2} (%)	D_0 (μm)	D_e (μm)	c	D_* (μm)	k_1 ($\times 10^{-10}$ m/s)	k_2 ($\times 10^{-10}$ m/s)
NC_P300	38.8	39.7	0.151	0.138	0.435	0.060	4.338	4.429
NC_S250	39.8	40.2	0.151	0.156	0.397	0.062	4.718	4.760
OCR3.3_P300	38.1	36.1	0.151	0.129	0.431	0.056	3.667	3.476
OCR4.0_S250	34.8	37.8	0.151	0.140	0.424	0.059	3.796	4.123

Notes: n_{*1} is the porosity calculated from e_{MIP} (Fig. 2a); n_{*2} is the porosity calculated from the corrected void ratio, $e_{MIP,c}$, according to e_0; k_1 and k_2 are the coefficients of permeability calculated with n_{*1} and n_{*2}, respectively.

5 Conclusions

The following conclusions can be obtained from this study: (i) The void ratio measured by MIP is often greater than that estimated from SEM image analysis, while the modal pore diameter acquired by MIP is much smaller than that obtained from SEM image processing. (ii) The influences of the over consolidation ratio (OCR) and the stress path on pore structures and permeabilities were observed. (iii) An improved permeability model based on the results of MIP tests was proposed and its capability of predicting the coefficient of permeability of fine-grained soils was verified.

References

Garcia-Bengochea, I., 1978. The relation between permeability and pore size distribution of compacted clayey silts: Interim report.

Garcia-Bengochea, I., Altschaeffl, A.G. and Lovell, C.W., 1979. Pore distribution and permeability of silty clays. Journal of the Geotechnical Engineering Division, 105(7), pp.839-856.

Lapierre, C., Leroueil, S. and Locat, J., 1990. Mercury intrusion and permeability of Louiseville clay. Canadian Geotechnical Journal, 27(6), pp.761-773.

Leonards, G.A., 1962. Foundation Engineering. New York : McGraw-Hill.

Xu, Y.H. and Pitot, H.C., 2003. An improved stereologic method for three-dimensional estimation of particle size distribution from observations in two dimensions and its application. Computer methods and programs in biomedicine, 72(1), pp.1-20.